

A matter of shape

Joaquin Garcia-Suarez¹

Institute of Civil Engineering, Institute of Materials, École Polytechnique Fédérale de Lausanne (EPFL), CH-1015 Lausanne, Switzerland

Abstract

I consider the fluid-mediated approach of a deformable elastic object (“indenter”) to a rigid surface at relatively low velocity. As a fluid is squeezed between the tip and the rigid substrate, lubrication pressures develop, which in turn deform the indenter leading edge. I study the influence of the tip geometry over the lubrication pressure distribution. “Low velocity” means that the approach happens slowly enough for the body to adapt quasi-statically to the transient viscous pressures triggered in the mediating fluid when squeezed. The salient geometrical simplification is that the indenter shape is axisymmetric, and its height profile goes like $\sim r^n$, r being the radial coordinate measured from the tip and n the exponent that controls the leading edge shape. I inquire if the distribution of pressures induced by the thin lubrication film forming before touchdown corresponds to the pressure distribution predicted by an equivalent “dry” contact mechanics problem. Results show striking resemblance for $n \leq 2$ while also partial ability to predict the pressure distribution for $n > 2$. Still, the analogy is deemed exceedingly insightful.

1. Introduction

One clarification upfront: this paper compares to similar geometrical settings with radically different mechanical properties’ distribution, see Figure 1. On one

¹Correspondence: joaquin.garciasuarez@epfl.ch

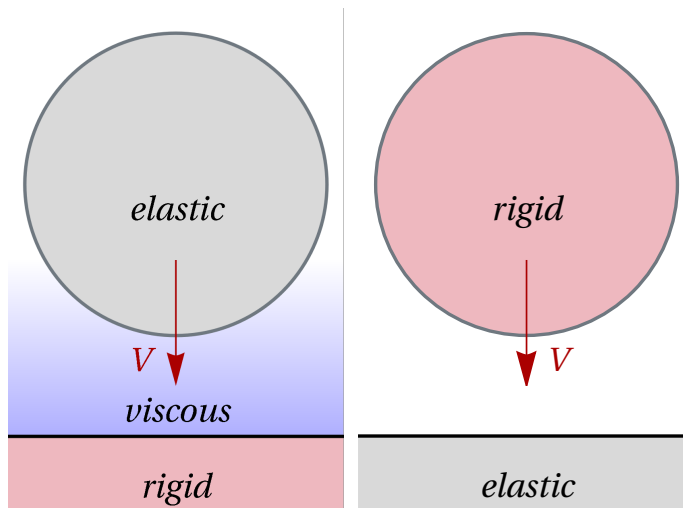


Figure 1: Actual problem (left) and analogy (right). Left: an elastic object moving towards a rigid substrate at “low” velocity (see Section 2.1) with fluid mediating between the two. Right: same geometrical setting and same velocity, but the fluid is removed and the stiffnesses are swapped. Both images represent the “approach” phase (we take it to correspond to $V < 0$), “contact” is considered when $V = 0$ and the “rebound” phase starts when $V > 0$.

hand, the classic indentation problem in which a finite rigid object impacts and deforms the surface of an elastic half-space. On the other one, the approach of a finite deformable object towards a rigid halfspace, mediated by a viscous fluid. In both cases, the finite object will be referred henceforth as “the indenter”.

One of the chief achievements of contact mechanics theory has been characterizing the distribution of pressure induced by simple indentation, i.e., when two bodies are pressured in contact by a normal force [1, 2, 3]. The pioneer work of Hertz on smooth locally-parabolic indenters was later generalized to consider any polynomial shape [1, 4]. Those results reveal the influence of shape over the contact pressure radial distributions, call it $p(r)$. Let the profile go like $\sim r^n$, for $n \leq 1$ there is a singularity at the symmetry axis, $n = 1$ represents the conical indentation, for $n = 2$ I recover the parabolic (Hertzian) indenter theory, for increasing $n > 2$ the maximum pressure moves away from the axis until reaching the flat punch case, featuring a pressure singularity at the edge of the contact

zone when $n \rightarrow \infty$.

Everything that has been said so far accounts neither for inertia nor for the presence of a fluid like air intervening between indenter and the substrate. Logically, there are many cases in which the influence of the mediating fluid can be ignored for most practical purposes, but that is not always the case. Experiments by Kolinski’s group at EPFL [5] showed that the air squeezed between the tip of a soft indenter and the substrate reacts by developing viscous pressures that in turn can significantly deform the tip of the approaching object. The deformed non-convex shape leads to a bubble of air being trapped between the tip and the substrate once contact is made, not at the tip but in an annulus. It has been shown [6, 7] that during the approach, once the viscous air response is triggered, the locally-parabolic indenter experiences a pressure distribution similar to the one predicted by Hertzian contact if the approach velocity is small enough. Hertz theory is a particular case of “dry” (no lubricating fluid) contact mechanics theory in which either the geometry of two finite bodies in contact is parabolic or one is while the other is an infinite rigid half-space.

Dry contact mechanics theory predicts not only the pressure distribution, but also the deformation (both vertical and radial) experienced by the indenter tip [6, 7]. This fact may appear bewildering: how is it possible that a framework that does not consider mediating fluid and assumes a rigid indenter deforming an elastic halfspace can predict the mechanical response when the stiffnesses of the indenter and halfspace swap and a lubricating fluid film is slipped in between? Figure 1 depicts both systems side by side.

In this paper, I intend to elucidate the “why” and explore how far the analogy can be run. To do so, the necessary (dry) contact mechanics theory and the numerical method to simulate the fluid-mediated approach [8] are reviewed in Section 2. The numerical and analytical results for four profiles (corresponding to $n = 1, 2, 3, 6$) are presented in Section 3. Those results are interrogated in Section 4, and Section 5 presents conclusions and future work avenues.

2. Methods

2.1. Dry impact

Consider an elastic halfspace indented by a rigid object (Figure 1 right). The impact indentation problem is equivalent to the static one when the total force being applied on the indenter is replaced by its inertia, which must be absorbed by the strain energy associated to the deformation of the body being indented. This setting assumes that the characteristic time of wave propagation in the solid is much shorter than the characteristic time of the viscous approach, so transient inertial effects in the solid can be neglected. More on this point in the next section. The compendium by Popov and colleagues [1] includes the general solution for an indenter whose height variation is given by a monomial r^n . They also notice that the pressure distribution developing under the indenter features the maximum at the center ($r = 0$) if $n \leq 2$, while the peak pressure moves the closer to the contact edge the higher the exponent $n > 2$.

The exact solution of the mixed-boundary value problem [2] yields the fields of interest (surface pressure, surface displacement...) in terms of integrals that can be evaluated for the different profiles. To obtain the results for different geometries in the dry case, I follow Sneddon [4]: his version of the integrals are evaluated symbolically in Mathematica [10]. For further reassurance, numerical solutions are also obtained using Tamaas [9]. Tamaas is a boundary element code optimized for contact mechanics problems.

Consider an indenter of mass m impacting a rigid surface. The deformation $\delta(t)$ (indentation depth) during contact is related to the elastic force $F(t)$, given by contact mechanics theory [1]:

$$F(t) = E^* \frac{2n}{n+1} \left[\frac{\kappa(n)}{2k} \right]^{1-n} \delta^{n+1}, \quad (1)$$

where:

- E^* is the effective Young's modulus, defined as $E^* = \frac{E}{1-\nu^2}$, with E being the Young's modulus and ν the Poisson's ratio of the material.

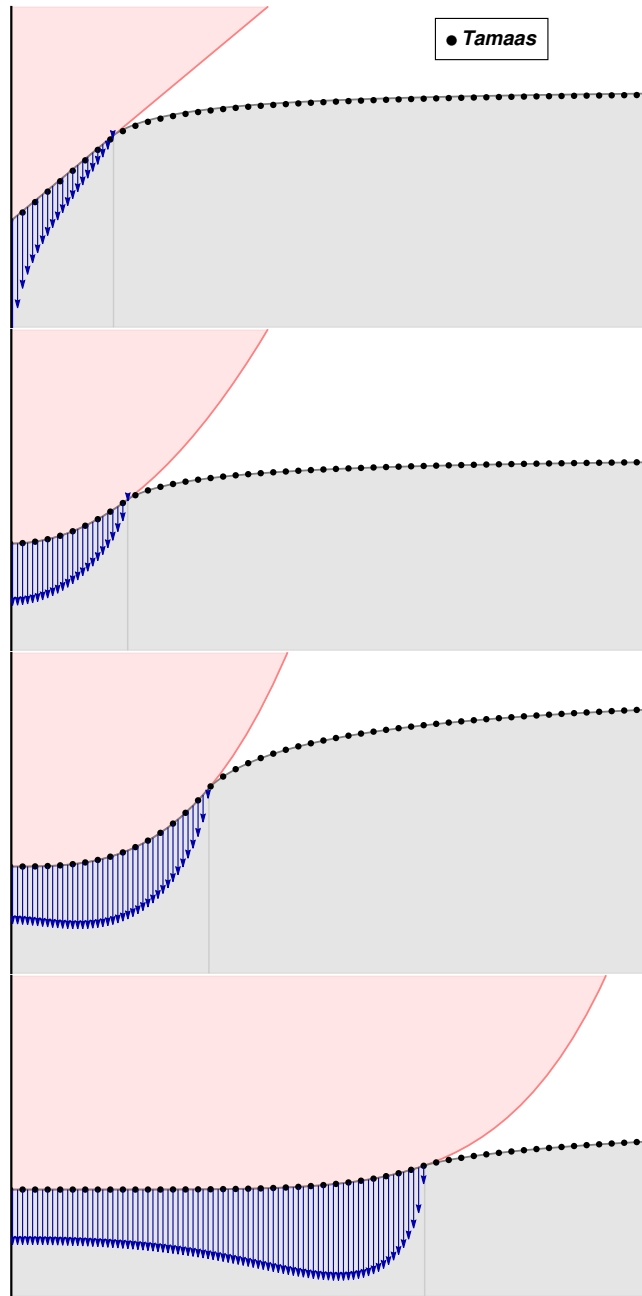


Figure 2: From top to bottom: dry indentation setting for linear, parabolic, cubic and hexic tip shapes. The pressure profiles shown are obtained from Tamaas simulations [9]. The deformed halfspace surface is represented by the analytical solution [4] with superimposed dots being the numerical Tamaas results. The darker vertical mark represents a , the contact radius.

- The function $\kappa(n)$ depends on the gamma function [1].
- k is the geometric constant of the indenter, such that the profile is written as $f(r) = r^n/2k$, the units being a function of the exponent.
- $\delta(t)$ is the indentation depth (always positive during contact).

Assuming that the wave propagation over the full object happens much faster than the characteristic time associated to the build-up of lubrication pressures in the thin film [7], applying Newton's second law in the vertical direction gives:

$$m\ddot{\delta}(t) = -F(t), \quad (2)$$

from this balance, one can also assess the energy conversion from kinetic to elastic energy. The dry-contact theory delivers the value of the maximum depth:

$$\delta_{\max} = \left(\frac{[\kappa(n)/2k]^{1/n}(2n+1)(n+1)mV_0^2}{4n^2E^*} \right)^{\frac{n}{2n+1}}. \quad (3)$$

The corresponding maximum contact radius is

$$a_{\max} = (2\delta_{\max}k)^{1/n}. \quad (4)$$

It is easy to recover the Hertzian (parabolic indenter) case [6] fixing $k = R$ and $n = 2$.

2.2. Fluid-mediated approach of indenter to smooth substrate

Analyzing this phenomenon (Figure 1 left) requires suitable descriptions of the indenter deformation (elasticity) and the viscous response of the air (lubrication). This letter is restricted to the quasi-static case, meaning that the characteristic time of the viscous phase of the approach is much longer than the characteristic time associated to wave propagation over the indenter tip [7]. This allows to borrow the numerical implementation by V. Bertin [6] of the implicit solver proposed in Ref. [8], featuring an efficient discretization scheme of the solid-fluid interaction problem based on the fundamental solution proposed by David et al. [11] and a finite-difference discretization for Reynolds lubrication equation, elegantly implemented in a concise

Python code. The slightly modified version used here only adds the possibility of changing the indenter shape; the original code can be accessed at <https://github.com/vincent-bertin/elastohydrodynamic-bouncing>.

The lubrication equations is:

$$r \frac{\partial h(r, t)}{\partial t} = \frac{1}{12\eta} \frac{\partial}{\partial r} \left(r h^3(r, t) \frac{\partial p(r, t)}{\partial r} \right), \quad (5)$$

where:

- $h(r, t)$ is the film thickness as a function of the radial coordinate r and time t .
- η is the dynamic viscosity of the fluid.
- $p(r, t)$ is the pressure field within the thin film.

The relative height depends on the shape of the profile and the deformation induced by the lubrication pressures. The profile is expressed as

$$h(r, t) = D(t) + \frac{r^n}{2k} - w(r, t), \quad (6)$$

where $D(t)$ represents the vertical position of the center point and w is the elastic vertical deformation, which is computed using a kernel [11]:

$$\begin{aligned} w(r, t) &= -\frac{4}{\pi E^*} \int_0^\infty \mathcal{M}(x, r) p(x, t) dx \\ &= -\frac{4}{\pi E^*} \int_0^\infty \frac{x}{x+r} K \left(\frac{4xr}{(x+r)^2} \right) p(x, t) dx, \end{aligned} \quad (7)$$

where p is the pressure distribution acting over the leading edge of the indenter and K is the complete elliptic integral of the first kind.

Following Ref. [6], I choose the characteristic values of the problem to be those furnished by contact mechanics. Their explicit form in terms of the physical parameters depends on the exponent n . Assuming that the undeformed profile shape is given as $f(r) = r^n/2k$, they have the form below in all cases independently of exponent. I also include the only dimensionless group that

appears, the Stokes number.

$$\text{Characteristic vertical length [1]: } \mathcal{H} = \left(\left(\frac{\kappa(n)}{2k} \right)^{1/n} \frac{(2n+1)(n+1)}{4n^2} \frac{mV_0^2}{E^*} \right)^{\frac{n}{2n+1}} \quad (8a)$$

$$\text{Characteristic radial length: } \mathcal{L} = (k\mathcal{H})^{1/n} \quad (8b)$$

$$\text{Characteristic pressure: } \mathcal{P} = \frac{2E^*}{\pi} \frac{\mathcal{H}}{\mathcal{L}} \quad (8c)$$

$$\text{Characteristic time: } \tau = \frac{mV_0}{E^* \mathcal{L} \mathcal{H}} \quad (8d)$$

$$\text{Stokes number: } \text{St} = \frac{\tau \mathcal{P} \mathcal{H}^2}{12\eta \mathcal{L}^2} \quad (8e)$$

These scales are selected purposefully to minimize the number changes needed to generalize the solver implementation that V. Bertin used to analyze parabolic indenters [6]. They guarantee that both sides of each dimensionless equation are $\mathcal{O}(1)$, except for the lubrication equation, eq. (5), where the Stokes number appear in its right-hand member.

Let us quickly comment on the meaning of some of the scales and on the significance of the Stokes number. \mathcal{P} represents the elastic stress associated to a characteristic strain, provided that \mathcal{H} and \mathcal{L} characterize the vertical and radial deformation respectively. τ is the characteristic time associated to the elastic forces decelerating the approaching object. Finally, the Stokes number, St , represents the ratio between elastic and viscous pressures over the timescale of the approach, i.e., the timescale associated to the complete deceleration of the object prior to rebound. Since the elastic pressures are linked to the complete deceleration (“dry impact setting”, prior subsection), the latter sets the scale for both geometrical length scales and time scale. This means that the St magnitude is $\gg 1$ given the rest of parameter values. In other words, the global indenter inertia would define the overall elastic deformation, a pre-assumption of the dry impact/contact setting (Section 2.1). This is, however, misleading. Over shorter timescales, the St must be $\mathcal{O}(1)$, meaning that the viscous pressures are the ones in charge of *locally* decelerating the approach and deforming the indenter, even though the *global* approach-contact-rebound process happens over a much

longer timescale. This is how these two facts are reconciled in practical terms: the simulations are run on the global timescale, starting at a height \mathcal{H} from the interface, imparting an initial velocity V_0 , running until the velocity of the object changes sign (approach ends, rebound starts); simultaneously the timestep is chosen small enough so as to resolve the timescale over which the viscous forces in the fluid locally balance the leading edge inertia.

3. Results

The time presented in the results is re-scaled so that $t = 0$ corresponds to the moment in which the tip of the indenter would contact the rigid substrate in the absence of intervening fluid. All the simulations correspond to $St = 1000 \gg 1$.

Figure 3 shows numerical pressure distribution at different times (solid lines) and compares it with the “contact mechanics analogy” (dashed lines). The analogy is computed using the analytical solution that gives pressures as a function of indentation depth, but using as indentation depth the numerical records of impactor deformation. For instance: in the parabolic case $f(r) = r^2/2R$, the pressure distribution using the analogy is $p(r, t) = 2E^*/\pi(R\delta_{\text{num}}(t) - r^2)^{1/2}$ where δ_{num} is the deformation, at time t , at the center obtained from the simulation, i.e., $\delta_{\text{num}} = w(0, t)$.

There is a small general caveat: the pressure at the edge in all cases transitions smoothly to zero in this case, while in contact mechanics it does so sharply out of the contact zone [6].

Let us point out that the agreement is excellent for $n \leq 2$, for greater values of the exponent the pressure at the center is underestimated and the maximum value overestimated. Nevertheless, in the case $n > 2$ the orders of magnitude are well captured and the qualitative trend as well, remarkably the pressure peaks away from the edge, although the numerical distributions are much more constant around the center than what the analogy predicts.

I also tested the analogy without any recourse to numerical results. To do so, I used a “constant kinematic indentation” proportional to the approach velocity,

δ_{kin} : for $t < 0 \rightarrow \delta_{\text{kin}} = 0$, for $t > 0 \rightarrow \delta_{\text{kin}} = V_0 t > 0$ increasing at constant rate. To be specific, using the parabolic case again, the “kinematic” indentation was computed as $p(r, t) = 2E^* / \pi(RVt - r^2)^{1/2}$. Results are presented at Figure 4, they correspond to maximum pressure (no matter where the peak happens) in all cases but $n = 1$, because the pressure is singular; the finite pressure at $r = 0.04\mathcal{L}$ is monitored instead. In all cases there is a good match for short times, for $n \leq 2$ they seem to worsen. In all cases the kinematic approximation overpredicts the final pressure.

4. Discussion

When it comes to pressure, the distribution predicted by contact mechanics seems to match with numerical results at the end of simulation, i.e., only when inertia is depleted, regard again Figure 3. However, Figure 4, a simple kinematic approximation would not give the real penetration depth and hence neither the pressure distribution.

Based on the results presented in the previous section, I can conclude that the contact mechanics analogy is a valid method to assess the pressure distribution that develops during fluid mediated impact. It remains to explain why it works. I surmise that a symmetry argument as well as a well-known equivalence in contact mechanics [3] can clarify this. The equivalence states that the problem of two elastic finite bodies contacting is similar to one rigid body deforming an elastic halfspace. In practical terms, the thin film would behave as a symmetric indenter which is pushed in contact with the real one. The equivalence method also proposes ways to “redistribute” the deformation computed in the indenter-halfspace setting between the two finite objects. There is no elastic deformation in the thin film, so when redistributing the displacement field between the two objects, it has to go to the actual indenter in full.

Finally, let us highlight that these dimensionless results are independent of the Poisson’s ratio, as it only appears in the definition of E^* . The only dimensionless group is the Stokes number. This is a departure for results at

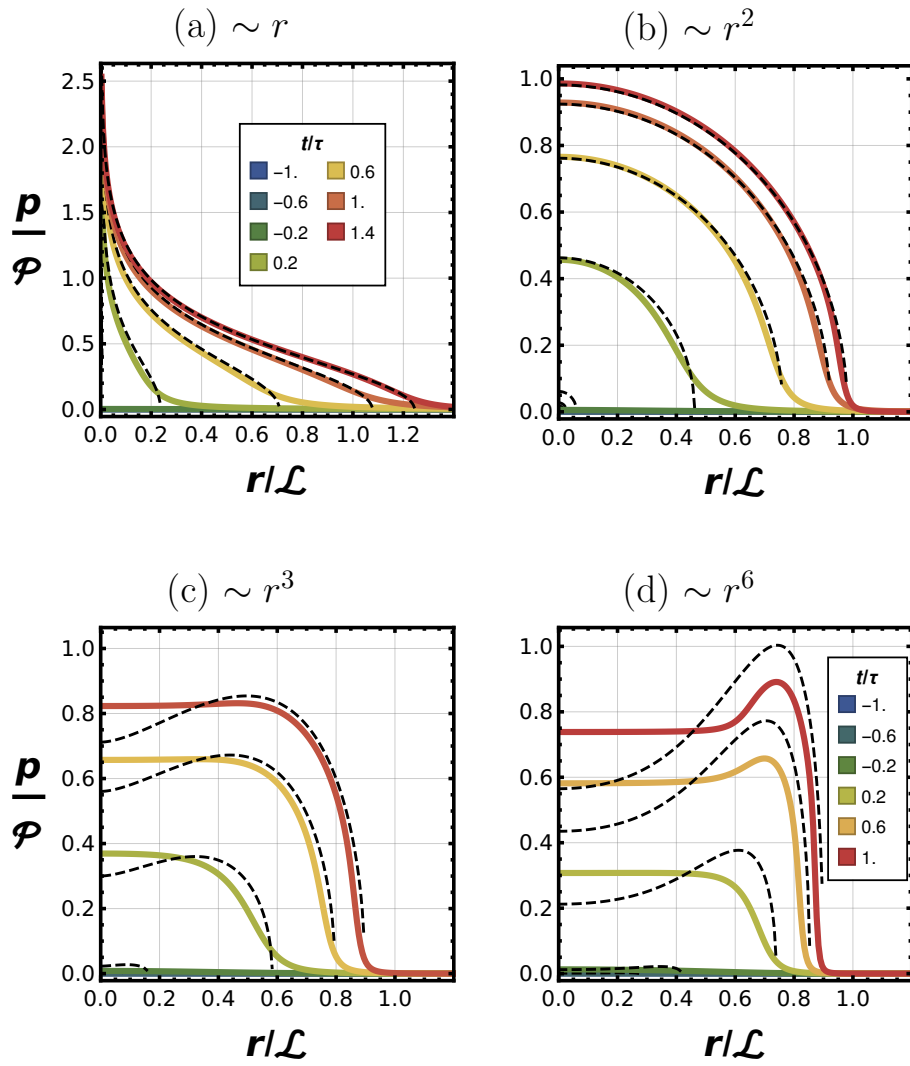


Figure 3: Pressure distribution over time at different times: simulation results and contact mechanics approximation based on numerical results for indentation. (a) Linear profile. (b) Parabolic. (c) Cubic. (d) Hexic.

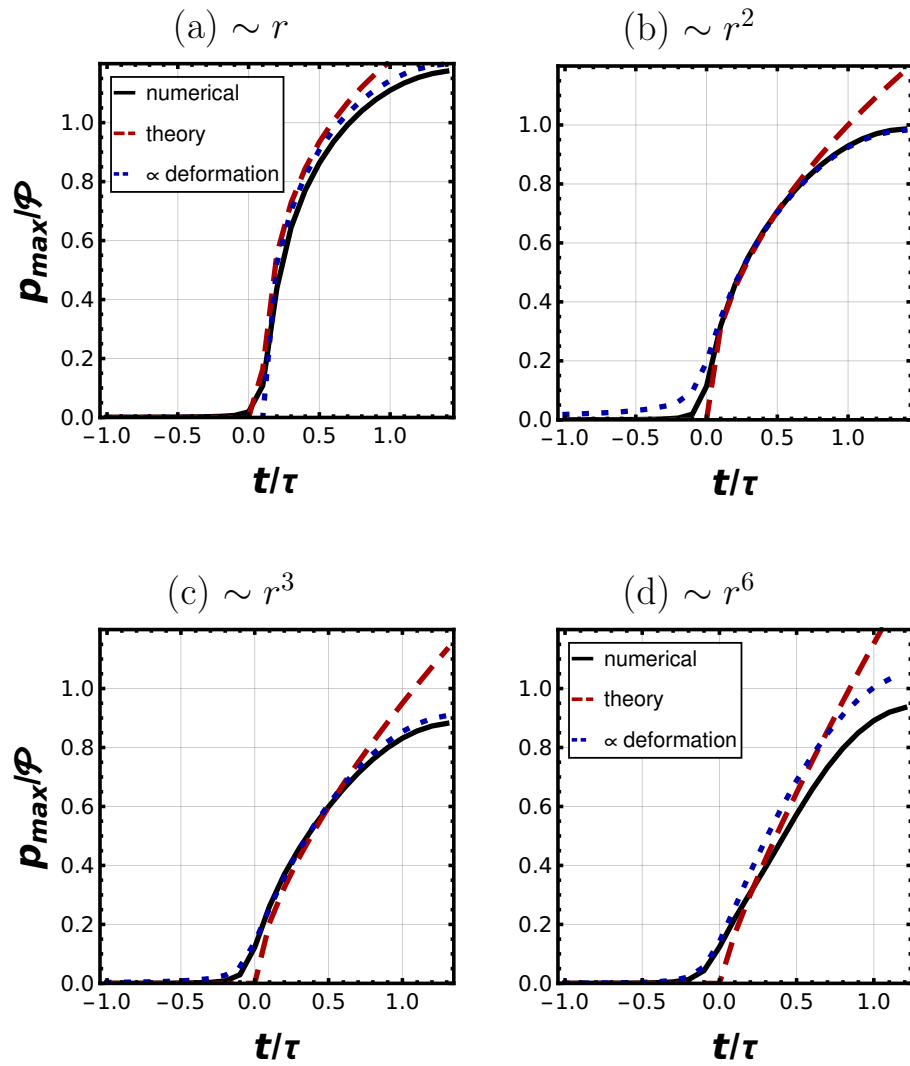


Figure 4: Maximum pressure over time according to numerical simulations, analogy using deformation numerical results and analogy using kinematic approximation to deformation. (a) Linear profile. (b) Parabolic. (c) Cubic. (d) Hexic.

higher approach velocities, which seem to change substantially as a function of the solid’s compressibility [7].

5. Final remarks

I have explored the pressure distribution that develops during fluid-mediated approach of elastic solids towards a rigid interface, finding that some of its traits can be predicted by “dry” (fluid-less) contact mechanics. The analysis has been restrained to low-velocity impacts, in which the solid response can be considered quasi-static.

When the low-velocity assumption is removed, one steps into the realm of fluid-mediated impact proper. Ref. [7] posited that a timescale competition gives rise to different regimes, τ_{impact} (characteristic time to fill the thin film) versus $\tau_{\text{propagation}}$ (characteristic time that it takes for elastic waves to propagate over the leading edge). As explained earlier, to assume quasi-static response in the solid, necessarily $\tau_{\text{impact}} \gg \tau_{\text{propagation}}$. Let us venture the hypothesis that the profile-controlling parameter k must also enter decisively into $\tau_{\text{propagation}}$, giving rise to physical shape-velocity correspondence in which the same dimensionless response can be achieved by either changing the velocity or the shape profile.

As another potential work avenues, let us mention the analysis of the details of the bubble geometry, as carried out in Ref. [6].

Acknowledgments

I am thankful to Prof. J.-F. Molinari and Mr. J. Bilotto (EPFL) for stimulating discussions. The support of the Swiss National Science Foundation via Ambizione Grant 216341 “Data-Driven Computational Friction” is gratefully acknowledged.

Data availability

All data will be made available openly before publication. In the meantime, all materials are available via correspondence with the author.

References

- [1] V. L. Popov, M. Heß, E. Willert, Handbook of contact mechanics: exact solutions of axisymmetric contact problems, Springer Nature, 2019.
- [2] J. R. Barber, Contact mechanics, Vol. 20, Springer, 2018.
- [3] K. L. Johnson, Contact Mechanics, Cambridge University Press, Cambridge, UK, 1985.
- [4] I. N. Sneddon, The relation between load and penetration in the axisymmetric boussinesq problem for a punch of arbitrary profile, International Journal of Engineering Science 3 (1) (1965) 47–57.
- [5] S. Zheng, S. Dillavou, J. M. Kolinski, Air mediates the impact of a compliant hemisphere on a rigid smooth surface, Soft Matter 17 (14) (2021) 3813–3819.
- [6] V. Bertin, Similarity solutions in elastohydrodynamic bouncing, Journal of Fluid Mechanics 986 (2024) A13.
- [7] J. Bilotto, J. M. Kolinski, B. Lecampion, J.-F. Molinari, G. Subhash, J. Garcia-Suarez, Fluid-mediated impact of soft solids, Journal of Fluid Mechanics 997 (2024) A35. doi:10.1017/jfm.2024.820.
- [8] Z. Liu, H. Dong, A. Jagota, C.-Y. Hui, Lubricated soft normal elastic contact of a sphere: a new numerical method and experiment, Soft Matter 18 (6) (2022) 1219–1227.
- [9] L. Frérot, G. Anciaux, V. Rey, S. Pham-Ba, J.-F. Molinari, Tamaas: a library for elastic-plastic contact of periodic rough surfaces, Journal of Open Source Software 5 (51) (2020) 2121.
- [10] S. Wolfram, The mathematica book, Vol. 4, Cambridge University Press Cambridge, 2000.
- [11] R. H. Davis, J.-M. Serayssol, E. J. Hinch, The elastohydrodynamic collision of two spheres, Journal of Fluid Mechanics 163 (1986) 479–497.

Appendix A. Non-dimensionalization and finite-difference discretization

The governing equations can be rendered dimensionless resorting to the characteristic values of the dry case Section 2.1. The dimensionless variables, using the scales in (8) become:

$$\tilde{r} = \frac{r}{\mathcal{L}}, \quad \tilde{w} = \frac{w}{\mathcal{H}}, \quad \tilde{h} = \frac{h}{\mathcal{H}}, \quad \tilde{D} = \frac{D}{\mathcal{H}}, \quad \tilde{t} = \frac{t}{\mathcal{H}/V_0}, \quad \tilde{p} = \frac{p}{\mathcal{P}}, \quad \tilde{V} = V/V_0. \quad (\text{A.1})$$

The new dimensionless eq. (5), eq. (6), eq. (2) and eq. (7) read as follows:

$$\tilde{r} \frac{\partial \tilde{h}(\tilde{r}, \tilde{t})}{\partial \tilde{t}} = \text{St} \frac{\partial}{\partial \tilde{r}} \left(\tilde{r} \tilde{h}^3(\tilde{r}, \tilde{t}) \frac{\partial \tilde{p}(\tilde{r}, \tilde{t})}{\partial \tilde{r}} \right), \quad (\text{A.2})$$

$$\tilde{h}(\tilde{r}, \tilde{t}) = \tilde{D}(\tilde{t}) + \frac{\tilde{r}^n}{2} - \tilde{w}(\tilde{r}, \tilde{t}), \quad (\text{A.3})$$

$$\frac{d\tilde{V}(\tilde{r}, \tilde{t})}{d\tilde{t}} = 4 \int_0^\infty \tilde{p}(\tilde{r}, \tilde{t}) \tilde{r} d\tilde{r}, \quad (\text{A.4})$$

$$\tilde{w}(\tilde{r}, \tilde{t}) = -\frac{8}{\pi^2} \int_0^\infty \tilde{\mathcal{M}}(\tilde{r}, \tilde{x}) \tilde{p}(\tilde{x}, \tilde{t}) d\tilde{x}. \quad (\text{A.5})$$

The discretization scheme applies a finite-difference method to solve the dimensionless equations.

1. Spatial and Temporal Discretization

A uniform spatial grid is defined as:

$$\tilde{r}_i = i\Delta\tilde{r}, \quad \text{for } i \in [0, N-1]$$

where $\Delta\tilde{r}$ is the grid size and N is the total number of radial points.

The temporal axis is discretized using a constant time step:

$$\tilde{t}^m = M\Delta\tilde{t}$$

where $\Delta\tilde{t}$ is sufficiently small (e.g., 10^{-3} or less) for numerical stability (resolving lubrication timescale).

2. Discretized Variables

Pressure, film thickness, and deformation are discretized as:

$$\tilde{p}(\tilde{r}, \tilde{t}) = \tilde{p}_i^m, \quad \tilde{h}(\tilde{r}, \tilde{t}) = \tilde{h}_i^m, \quad \tilde{w}(\tilde{r}, \tilde{t}) = \tilde{w}_i^m$$

Velocity and sphere position are given by \tilde{V}^m and \tilde{D}^m .

3. Discretized Thin-Film Equation

The thin-film equation (A4a) becomes:

$$\tilde{V}^{m+1} - \frac{\tilde{w}_i^{m+1} + \tilde{w}_i^m}{\Delta t} = \text{St} \left[\frac{(\tilde{h}_i^m)^3}{\tilde{r}_i} \frac{\partial \tilde{p}}{\partial \tilde{r}} \Big|_i^{m+1} + 3(\tilde{h}_i^m)^2 \left(\frac{n}{2} \tilde{r}_i^{n-1} - \frac{\partial \tilde{w}}{\partial \tilde{r}} \Big|_i^m \right) \frac{\partial \tilde{p}}{\partial \tilde{r}} \Big|_i^{m+1} + (\tilde{h}_i^m)^3 \frac{\partial^2 \tilde{p}}{\partial \tilde{r}^2} \Big|_i^{m+1} \right]$$

with film thickness:

$$\tilde{h}_i^m = \tilde{D}^m + \frac{\tilde{r}_i^n}{2} - \tilde{w}_i^m$$

4. Spatial Derivative Approximations

First-order and second-order derivatives are approximated as:

$$\begin{aligned} \frac{\partial \tilde{w}}{\partial \tilde{r}} \Big|_i^m &= \frac{\tilde{w}_{i+1}^m - \tilde{w}_i^m}{\Delta \tilde{r}}, \\ \frac{\partial \tilde{p}}{\partial \tilde{r}} \Big|_i^{m+1} &= \frac{\tilde{p}_{i+1}^{m+1} - \tilde{p}_i^{m+1}}{\Delta \tilde{r}}, \\ \frac{\partial^2 \tilde{p}}{\partial \tilde{r}^2} \Big|_i^{m+1} &= \frac{\tilde{p}_{i+1}^{m+1} - 2\tilde{p}_i^{m+1} + \tilde{p}_{i-1}^{m+1}}{\Delta \tilde{r}^2} \end{aligned}$$

5. Boundary Conditions

Symmetry at $\tilde{r} = 0$:

$$\frac{\partial \tilde{p}}{\partial \tilde{r}} \Big|_{\tilde{r}=0} = 0 \implies \tilde{p}_1^n - \tilde{p}_0^n = 0$$

Decay at large radius:

$$\tilde{p}_{N-1}^n = 0$$

6. Integral Equation of Elasticity

Elastic deformation \tilde{w}_i^m is computed using:

$$\begin{aligned} \tilde{w}_i^m &= -\frac{8}{\pi^2} \left[\tilde{p}_0^m \int_0^{\Delta r/2} \frac{x}{x + \tilde{r}_i} K \left(\frac{4x\tilde{r}_i}{(x + \tilde{r}_i)^2} \right) dx \right. \\ &\quad \left. + \sum_{j=1}^{N-1} \tilde{p}_j^m \int_{\tilde{r}_j - \Delta r/2}^{\tilde{r}_j + \Delta r/2} \frac{x}{x + \tilde{r}_i} K \left(\frac{4x\tilde{r}_i}{(x + \tilde{r}_i)^2} \right) dx \right] \end{aligned}$$

7. Newton's Second Law for the Indenter

Velocity and position updates:

$$\frac{\tilde{V}^{m+1} - \tilde{V}^m}{\Delta t} = 4 \sum_{i=0}^{N-1} \tilde{p}_i^{m+1} \tilde{r}_i \Delta \tilde{r}$$

$$\frac{\tilde{D}^{m+1} - \tilde{D}^m}{\Delta t} = \tilde{V}^{m+1}$$

The recasting of the equations into a linear system of equations (the unknown vector containing the values of surface deformation in the solid and the pressure in the fluid) that can be solved with standard numerical methods follows the scheme presented in [8].